DOI: 10.24850/j-tyca-14-04-08

Articles

Estimated potential erosion in the Papaloapan River: Modeling efficiency and uncertainty

Erosión potencial estimada en el río Papaloapan: eficiencia e incertidumbre en las modelaciones

Mayrén Alavez-Vargas[1], ORCID: https://orcid.org/0000-0001-9296-0815

Giovanni González-Celada[2], ORCID: https://orcid.org/0000-0002-1815-4978

Christian Birkel[3], ORCID: https://orcid.org/0000-0002-6792-852X

Roxana Fonseca[4]

José Agustín Breña-Naranjo[5], ORCID: https://orcid.org/0000-0002-9853-3109

[1]Consejo Nacional de Ciencia y Tecnología, Mexico City, Mexico, mayren.alavez@catie.ac.cr

[2]Instituto Privado de Investigación sobre Cambio Climático, Escuintla, Guatemala, gio.gonzalezw@gmail.com

[3]Departamento de Geografía y Observatorio del Agua y Cambio Global de la Universidad de Costa Rica, San José, Costa Rica, christian.birkel@ucr.ac.cr

[4]Instituto de Ingeniería de la Universidad Nacional Autónoma de México, Mexico City, Mexico, roxana.fonseca.rdz@gmail.com

[5]Instituto Mexicano de Tecnología del Agua, Jiutepec, Mexico, agustin_brena@tlaloc.imta.mx

Corresponding author: Mayrén Alavez-Vargas, mayren.alavez@catie.ac.cr

Abstract

Global knowledge on the consequences of changes in vegetation and land use in the phases of the hydrological cycle and soil quality is still incipient. This task is particularly challenging in tropical regions, where deforestation rates reach their highest reported levels and monitoring is limited. Such is the case of Mexico, where changes in coverage and water erosion affect more than half of the national territory. In this context, the SWAT model was used to study water erosion associated with variations in flow conditioned by the trajectory of change in vegetation cover in six periods, between 1986 and 2018, in two sub-basins of the Papaloapan River. Based on the combined evaluation of three efficiency and two uncertainty statistics, six of the ten calibrated periods showed good fitting in discharge simulation with KGE > 0.70 and P-factor > 0.70. In the medium term, the results showed a decrease in sediment yield in the two study sub-basins, possibly related to the recovery of the forests in the basins' headwaters. In spite of the good results of the simulations, the detailed analysis of the sources of uncertainty in regions with limited monitoring is as important as the validation with good-quality measured data, in order to improve the performance and reliability of the models and to support adequate decision-making.

Keywords: Erosion, flow, SWAT, deforestation, land use change, tropics, efficiency, uncertainty.

Resumen

El conocimiento global de las consecuencias del cambio de vegetación y uso de suelo en las fases del ciclo hidrológico y la calidad del suelo aún está en ciernes. Esta tarea es particularmente desafiante en las regiones tropicales donde las tasas de deforestación alcanzan los niveles máximos reportados y el monitoreo es limitado. Tal es el caso de México, donde el cambio de cobertura y la erosión hídrica afectan a más de la mitad del territorio nacional. En este contexto, se usó el modelo SWAT para estudiar la erosión hídrica asociada con las variaciones en el caudal condicionadas por la trayectoria de cambio de la cobertura vegetal en seis periodos entre 1986 y 2018 en dos subcuencas del río Papaloapan. Basados en la evaluación combinada de tres estadísticos de eficiencia y dos de incertidumbre, 6 de los 10 periodos calibrados mostraron buenos ajustes en la simulación de la descarga con KGE > 0.70 y P-factor > 0.70. Los resultados mostraron a mediano plazo una disminución en la producción de sedimentos en las dos subcuencas estudiadas, posiblemente relacionada con la recuperación de los bosques en las cabeceras de las cuencas. A pesar de los buenos resultados de las simulaciones, el análisis detallado de las fuentes de incertidumbre en regiones con monitoreo limitado es tan importante como la validación con datos medidos de buena calidad para mejorar el desempeño y la confianza de los modelos y soportar de forma adecuada la toma de decisiones.

Palabras clave: erosión, caudal, SWAT, deforestación, cambio de uso de suelo, trópicos, eficiencia, incertidumbre.

Received: 04/06/2020

Accepted: 29/01/2022

Introduction

Water erosion is a naturally occurring and anthropogenic process of the earth's surface, whose magnitude on a global scale is estimated to be in the range of 20–30 gigatons per year (FAO & ITPS, 2015). The highest rates of deforestation occur in the tropical regions of the Global South, (Borrelli *et al.*, 2017) promoted by the expansion of the agricultural frontier, the extraction of resources and/or growing urbanization Montes-León, Uribe-Alcántara, & García-Celis, 2011). During the last decade, transitions from forest cover to other land uses increased at a rate of 0.46 % in Latin America and the Caribbean (FAO, 2011) and of 0.3 % in Mexico (Blackman, Goff, & Rivera-Planter, 2018); both rates exceed the world average of 0.13 % (FAO, 2011). Compounded by human activity, water erosion in the tropics is exacerbated due to high-intensity seasonal rainfall regimes (Rangel, Jorge, Guerra, & Fullen, 2019). Thus, more than 60 % of Mexican soil presents some level of erosion due to water degradation, which worsens at an average annual rate of 0.5 % (Borrelli *et al.*, 2017). These serious water erosion processes become especially acute in the stages subsequent to changes in cover and land use (Cardoza-Vázquez *et al.*, 2007; Bolaños-González *et al.*, 2016).

Changes in coverage affect environmental services, the water cycle and the soil at multiple spatial and temporal scales, depending on the physiography of the basin, climate variability, and the trajectory of use of the studied territory (Martinez, Guyot, Filizola, & Sondag, 2009; Arheimer & Lindström, 2019). For example, vegetation and land use are important factors in the hydrological behavior of basins, since they determine surface and subsurface runoff generation processes Arheimer & Lindström, 2019; Couto *et al.*, 2019; Liu, Zhang, Kou, & Zhou, 2017). At a regional scale, the volume of runoff and transported sediments increases, causing morphological alterations to the river network and the hydrological regime of the basins, and there is a higher risk of flooding in the plains (Chotpantarat & Boonkaewwan, 2018; Wang, Ge, Yu, Wang, & Xu, 2017; Yang *et al*., 2018).

In tropical countries, hydrological monitoring is performed with scanty measurement networks (Vörösmarty, Lévêque, & Revenga, 2005), resulting in limited historical records (Carvalho, 2019; Delmas, Cerdan, Cheviron, & Mouchel, 2011; Warrick, 2014). The convergence of historical data scarcity, the need of information for decision-making, advances in computing technologies, and the production of scientific knowledge contribute to the application of hydrological models as the most widely used tools for research, planning, and environmental management (Fakhri, Dkohaki, Eslamian, Fazeli-Farzani, & Reza-Farzaneh, 2014; Jajarmizadeh, Harun, & Salarpour, 2012; Jørgensen & Fath, 2011). Similarly, geographic information systems have enhanced the management of large amounts of information, yielding advantages such as the display of spatially distributed results and the generation of scenarios (Alatorre & Beguería, 2009; Goodchild, 1996).

The Soil and Water Assessment Tool (SWAT) is a physically based conceptual model that estimates water, sediment, nutrients, pollutants, and pathogens at basin level from spatially distributed data on topography, soil, vegetation and land use, management practices, and climate (Douglas-Mankin, Srinivasan, & Arnold, 2010). The operation of this model is defined by the principles of mass and momentum: the former is related to the balance of water, sediments, nutrients or contaminants, and the latter focuses mainly on the displacement of these flows through the drainage network of the basin. The main areas of application of the SWAT model include water quality in relation to non-point source contamination, sediment production, runoff simulation, and the hydrological impacts of environmental change (Wang *et al*., 2019).

In the SWAT model, the dynamics of the variables of interest is modeled from spatially distributed physiographic, climatic, and anthropic input data, so that it is useful in ungauged basins or in the evaluation of long-term scenarios based on variations of some of the input variables (Neitsch, Arnold, Kiniry, & Williams, 2011). In this case study, it will be based on changes in coverage and land use. The use of the SWAT model in countries with limited monitoring is widespread. Across regions of East Africa, Guzha, Rufino, Okoth, Jacobs and Nóbrega (2018) identified 15 studies that used SWAT to assess the impact of land use on surface runoff, discharge, and baseflow. For their part, Tan, Gassman, Srinivasan, Arnold and Yang (2019) reviewed 126 cases that studied different issues of land use change, climate change, management practices, and/or water quality with SWAT in Southeast Asia.

In the Papaloapan River basin, Bello, Gómez, Magaña, Graizbord and Rodríguez (2009), and Ruiz-Fernández *et al*. (2014) pointed out that siltation problems in the system of lagoons and wetlands of the lower basin are associated with a large amount of sediment transported by tributaries upstream during the last forty years. Pérez-Vega and Ortiz-

Pérez (2002) established a positive relationship between the increase in the runoff of the sub-basins of the San Juan and Tesechoacán rivers and the increase in deforestation in the Papaloapan River basin between 1973 and 1993.

From the standpoint that environmental processes are historical —as a product of a historical legacy but also the result of a combination of variables in the present Reid 1998; Verstraeten Lang, & Houben, 2009)— and susceptible to research with available resources, the SWAT model was used to reconstruct the trajectory of the potential erosion associated with land use change with the following specific objectives:

1. To estimate water erosion and flow variations with respect to changes in land use and cover from 1985 to 2018 in two sub-basins of the Papaloapan River.
2. To estimate the spatial distribution of the erosion potential in the study area.

Study area and databases

The sub-basins of the San Juan (SJN) and Tesechoacán (TES) rivers constitute 26 % of the 46 720 km^2 of the total area of the Papaloapan River basin, which is located on the slope of the Gulf of Mexico between 19° N 97° W and 17° N 94° W (Figure 1).

Tecnología y Ciencias del Agua

OPEN ACCESS

Check for updates

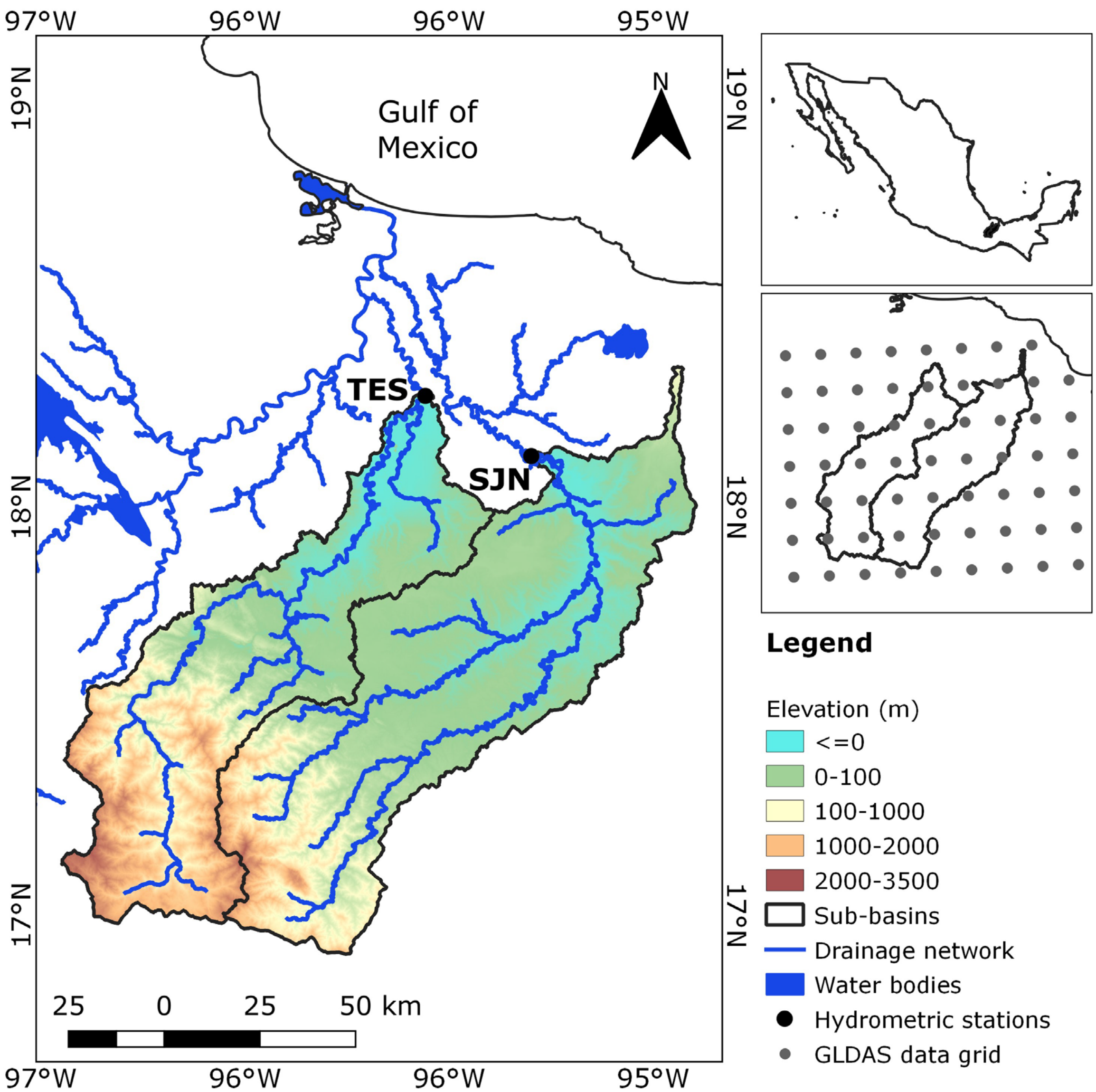

Figure 1. Location of the study sub-basins (upper right) with elevation (left) and data grid from the Global Land Data Assimilation System (GLDAS) (lower right).

About 55 % of the study area has slopes that are less than 15 % steep and 45 % of the remaining area has slopes steeper than 15 % (FAO, 2009). Using the Köppen classification modified for Mexico by García (2004), three climate groups are identified in the region: (A) tropical rainy, in the plains close to sea level; (B) dry with summer rains and (C) humid temperate in the high basins (up to 3 400 masl). Twelve types of vegetation and land use were identified, grouped into five classes: Temperate forests, tropical forests, scrub and chaparral areas, pastures, and agriculture (Alavez-Vargas, Birkel, Corona, & Breña-Naranjo, 2021) (Figure 2).

Tecnología y Ciencias del Agua

OPEN ACCESS

Check for updates

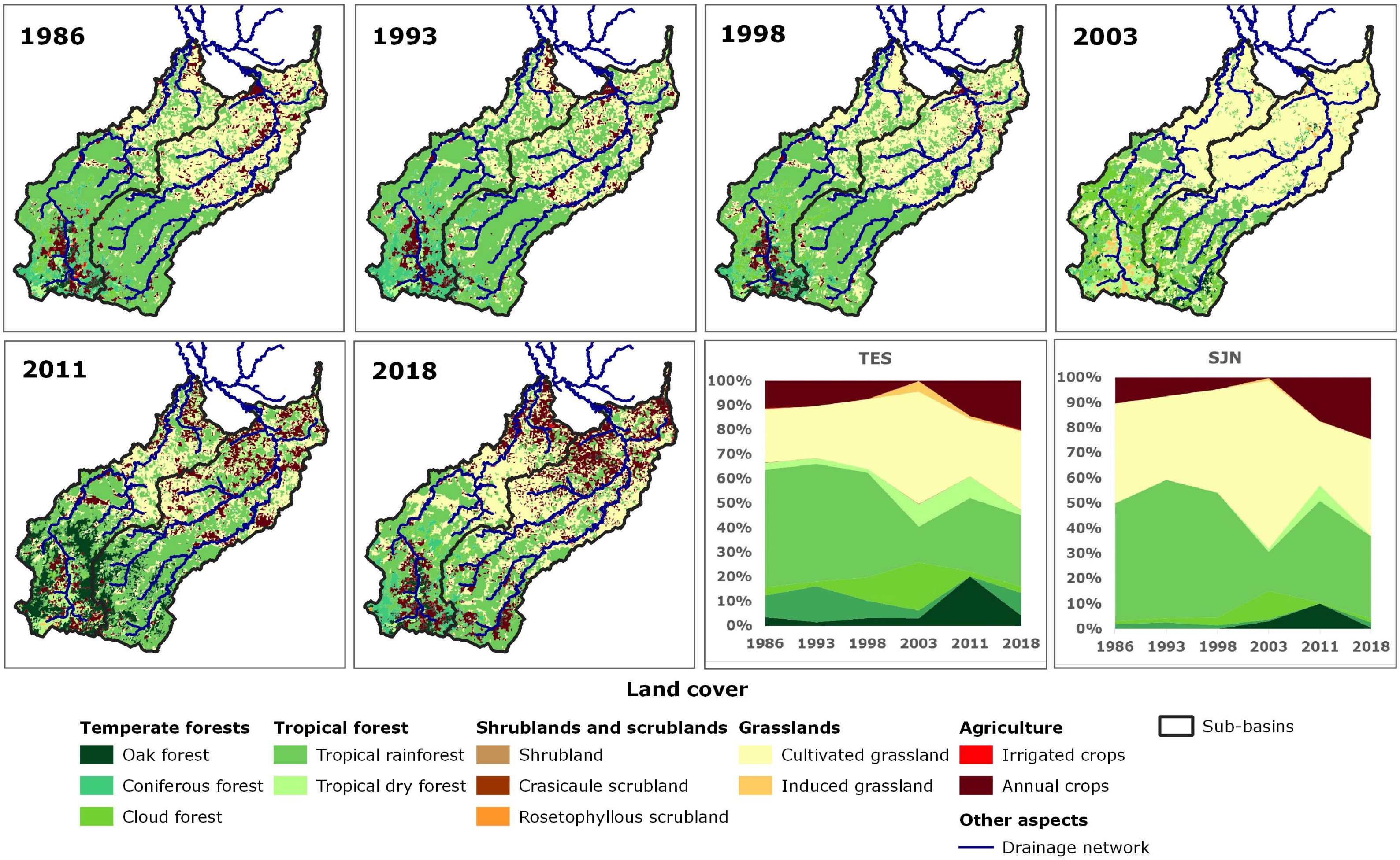

Figure 2. Vegetation and land use from 1986 to 2018, geographical representation and percentages by study sub-basin.

The Air Shuttle Radar Topographic Mission (SRTM) digital elevation model, with a spatial resolution of 90 m, was used in this study (Jarvis, Reuter, Nelson, & Guevara, 2008). This raster information was reclassified into slope ranges, based on the geomorphology of the basin and FAO's classification (FAO, 2009) in order to create two classes: 0–15 % and steeper than 15 %. The vector sets corresponding to the drainage network (INEGI, 2010) come from the thematic geospatial information produced by the National Institute of Statistics, Geography and Informatics (INEGI) of Mexico. The edaphological information required by the model was derived from the vector sets related to the edaphological units (INEGI, 2007) and the edaphological profiles (INEGI, 2013), in addition to two software packages for estimating other characteristics not available in the sources previously consulted: using the Soil Water Characteristics software (Saxton & Rawls, 2006), the saturated hydraulic conductivity, the apparent density, and basic infiltration were assessed, whereas the hydrological soil groups were identified using the NumCur 10 IE software. The types of vegetation and land use were classified according to the procedure described in Alavez-Vargas *et al*. (2021) from Landsat images downloaded from Google Earth Pro (Wuthrich, 2006), processed in QGIS v. 3.4.5 Madeira (QGIS Development Team, 2019), for the years 1986, 1993, 1998, 2003, 2011, and 2018 (Figure 2) and subsequently reclassified according to the nomenclature used by the model. Daily (Li, Beaudoing, & Rodell, 2018) and tri-hourly (Beaudoing & Rodell, 2015; Beaudoing & Rodell, 2016) temperature, precipitation, wind speed, and solar radiation data, with an approximate spatial resolution of 25 km^2, for the period 1980–2018, were obtained from the Global Terrestrial Data Assimilation System (GLDAS) portal (Rodell *et al*., 2004) in a 63-point grid over the study area (Figure 1). Finally, the daily flow measurements from 1985 to 2014 were taken from the National Surface Water Data Bank (BANDAS for its acronym in Spanish) (Conagua, 2017). The products, resolutions, and sources consulted to obtain the data of the ten biophysical and climate variables collected are summarized in Table 1.

Table 1. Characterization of input data.

Variable	**Product and temporal resolution**	**Resolution**	**Source**
Digital Elevation Model	SRTM, raster format	90 m	Jarvis *et al.* (2008)
Water network	Hydrographic network, vector format	Scale 1:50,000	INEGI (2010)
Edaphology	Edaphological units	Scale 1:250 000	INEGI (2007)
	Edaphological profiles	Scale 1:250 000	INEGI (2013)
Vegetation	Landsat images, raster format, years 1986, 1993, 1998, 2003, 2011, 2018	30 m	Wuthrich (2006)

Variable	Product and temporal resolution	Resolution	Source
Temperature	GLDAS Noah Land Surface Model L4 V 2.0 Period: 1980-01-01 a 2010-12-31	Three hours, 0.25º x 0.25º	Beaudoing y Rodell (2015)
	GLDAS Noah Land Surface Model L4 V 2.1 Period: 2011-01-01 a 2018-12-31	Three hours, 0.25º x 0.25º	Beaudoing y Rodell (2016)
Precipitation	GLDAS Catchment surface Model L4 V 2.0 Period: 1980-01-01 a 2010-12-31	Daily 0.25º x 0.25º	Li *et al.* (2018)
Wind velocity			
Solar radiation	GLDAS Noah Land Surface Model L4 V 2.1 Period: 2010-01-01 a 2018-12-31	3 horas 0.25º x 0.25º	Beaudoing y Rodell (2016)
Hydrometric stations	Location of the hydrometric stations Garro (Tesechoacán River) and Cuatotolapan (San Juan River)		Conagua (2017)
Measured flow	BANDAS daily records Period 1985-01-01 a 2014-12-31	Daily	Conagua (2017)

Methods

SWAT model configuration

SWAT modeling consists of five stages (Figure 3). Initially, the digital elevation model and the river network guide the delimitation of the study sub-basins. Subsequently, the variables with which the model defines the hydrological response units (HRUs) are incorporated: slope, soil type, vegetation type, and land use. These first two stages, therefore, focus on the physical delimitation of the units (sub-basins) and sub-units of analysis (HRUs) by which, in the next stage, the information of the input variables is grouped and the responses of the components of the water balance (Equation 1) and the variables of interest are calculated (erosion in this case, Equation 2) (Neitsch *et al*., 2011).

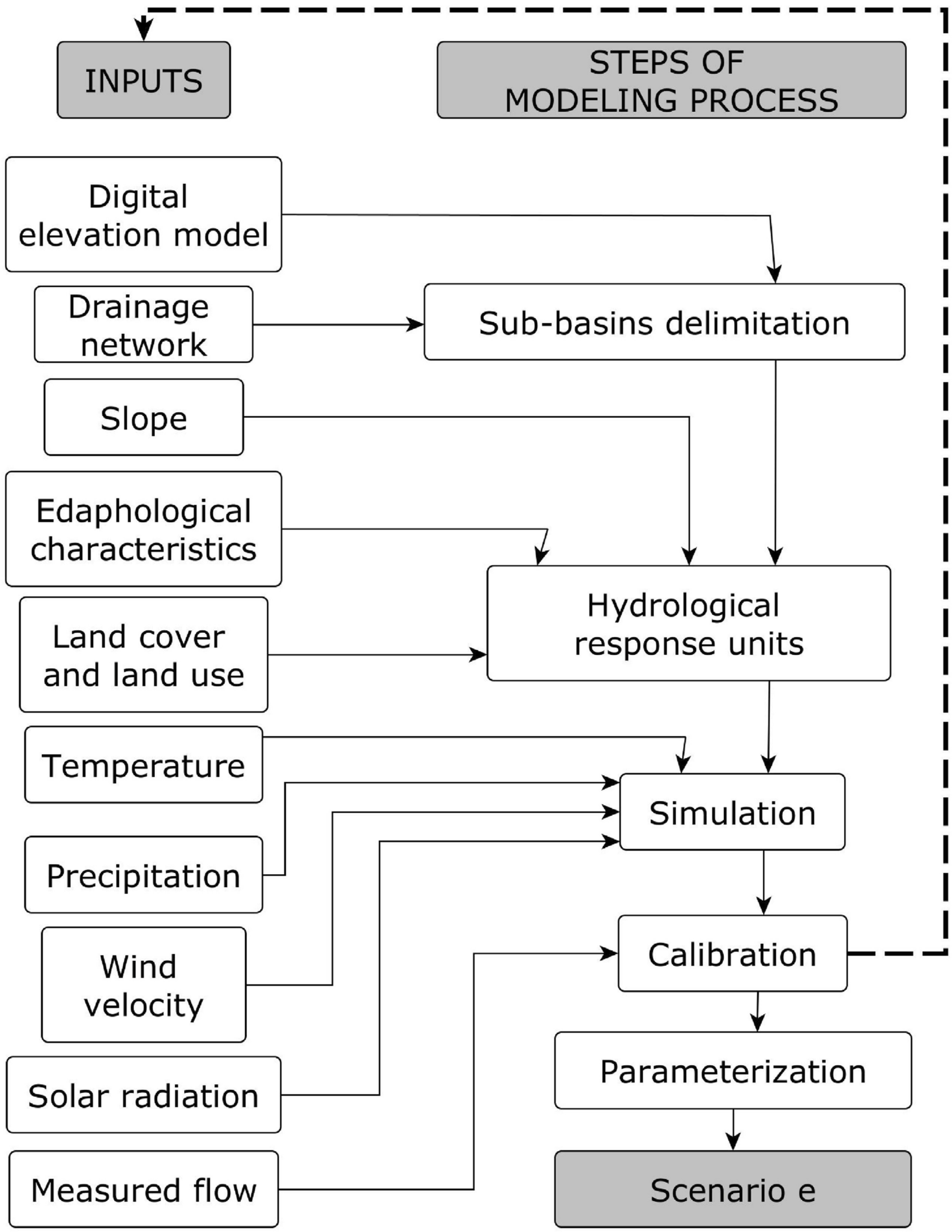

Figure 3. SWAT modeling workflow: input data preparation and model application and calibration.

In the third stage, the model was fed with the following climate variables: precipitation, maximum and minimum temperatures, solar radiation, and wind velocity. Together, these variables represent the amounts of water and energy that govern the water balance. Specifically, these data are used by the model to solve the water balance equation (Equation 1) at HRU scale per sub-basin (Neitsch *et al.,* 2011):

$$SW_t = SW_0 + \sum_{i=1}^{t}\left(R_{day} - Q_{surf} - E_a - W_{seep} - Q_{gw}\right) \quad (1)$$

Where SW_t: final soil water content (mm), SW_0: initial soil water content on day *i* (mm); *t*: time in days; R_{day}: precipitation on day *i* (mm); Q_{surf}: surface runoff on day *i* (mm); E_a: evapotranspiration on day *i* (mm); W_{seep}: percolation on day *i* (mm), and Q_{gw}: return flow on day *i* (mm).

In turn, erosion in HRUs by sub-basin is calculated with the Modified Universal Soil Loss Equation (MUSLE, Equation (2)) (Williams, 2012):

$$sed = 11.8\left(Q_{surf} \times q_{peak} \times area_{hru}\right)^{0.56} \times K_{USLE} \times C_{USLE} \times P_{USLE} \times LS_{USLE} \times CFRG \quad (2)$$

Where *sed*: daily produced sediment (ton); Q_{surf}: daily surface runoff sheet (mm ha^{-1}); q_{peak}: peak flow ($m^3\ s^{-1}$); $area_{hru}$: HRU area (ha);

K_{USLE}: soil erodibility factor; C_{USLE}: plant cover and management factor; P_{USLE}: support practices factor; LS_{USLE}: topographic factor, and *CFRG*: soil fragmentation factor.

The result of the third stage is the initial simulation of the scenario in turn. This simulation is calibrated with data of the analyzed variables, as described in the following section.

Initial simulation and calibration

This study was carried out in QGIS, version 2.6.1 Brighton (QGIS Development Team, 2014) with the QSWAT extension, version 1.8 (Dile, Srinivasan, & George, 2019). The input data was prepared in the format required by the software for the calculation of the different variables involved in equations 1 and 2. The equations given by default by the model were used, (see Arnold *et al*., 2011) except for evapotranspiration, which was calculated with the Hargreaves, Hargreaves and Riley (1985) method. The values of the physical parameters (i.e., the elevation, the drainage network, the slope and the edaphological characteristics) were constant for the six periods assessed in each sub-basin. Vegetation covers and land use were specific for each scenario. The climate information introduced had a daily resolution. Due to the absence of databases on soil conservation practices in the study area, the P_{USLE} support practices factor was considered equal to 1, i.e., without conservation practices.

For the period from 1986 to 2018, six models were carried out per sub-basin, corresponding to the periods defined by the vegetation and land-use scenarios, as shown in Table 2. The irregularity of the assessed intervals is due to the methodological decisions made to ensure the mosaic of images of the best possible quality to characterize the cover and land use in each scenario.

Table 2. Periods of warming, modeling and calibration in the three studied sub-basins.

Vegetation and land use scenario	Modeling	Warm-up	Monthly flow calibration
1986	1982-1986	1982-1983	1985-1986
1993	1985-1993	1985-1986	1987-1993
1998	1992-1998	1992-1993	1994-1998
2003	1997-2003	1997-1998	1999-2003
2011	2002-2011	2002-2003	2004-2011
2018	2010-2018	2010-2011	2012-2014

For each modeling, a warm-up period of two years was defined, as suggested by Arnold *et al*. (2012). The modeling had a monthly time scale.

Flow calibration was performed with 30 years of observed data (1985–2014) at the hydrometric stations of the San Juan and Tesechoacán sub-basins. The simulated erosion was not calibrated due to the absence of erosion data in the three study sub-basins.

The sensitivity, uncertainty, and calibration analyzes of the models were carried out following the recommendations of Abbaspour, Vaghefi and Srinivasan (2017) with the SUFI-2 algorithm available in the SWAT-CUP software (Abbaspour, 2015). The SUFI-2 algorithm focuses on the search for the group of parameters with the best fit and least uncertainty regarding the data observed by means of sampling by the Latin hypercube method (Beven, 2012), with the aim of fulfilling two conditions: that more than 90 % of the data be located in the 95 percent prediction uncertainty (95PPU) area and that the proportion in the average difference between the limit values of the 95PPU and the standard deviation be less than 1 (Abbaspour, Johnson, & van Genuchten, 2004).

For each scenario and sub-basin, at least three iterations of 600–1000 simulations were carried out. The Kling Gupta Efficiency (KGE) criterion was used as the objective function, and the Nash-Sutcliffe efficiency statistics (NSE), the percentage of bias (PBIAS) and the coefficient of determination (R^2) were also performed.

The Kling Gupta criterion evaluates the goodness of fit of the model by calculating the Euclidean distances between the correlation, the bias and the variability of the simulated value with respect to the observed value (Equation (3) and Equation (4)) as an alternative to the Nash Sutcliffe criterion, which takes as reference the difference of 1 minus the ratio of the mean squared error and the variance (Equation 5) to show the proportion of the variability of the observations explained by the simulation (Gupta, Kling, Yilmaz, & Martínez, 2009):

$$KGE = 1 - ED \tag{3}$$

$$ED = \sqrt{(r-1)^2 + (\alpha - 1)^2 + (\beta - 1)^2} \tag{4}$$

Where *ED* is the Euclidean distance from the ideal point, *r* is the linear correlation coefficient between simulated and observed data, α is the variability given by the ratio between the standard deviations of the simulated and observed data, and β is the bias given by the ratio between the simulated and observed mean flows:

$$NSE = 1 - \frac{\sum_{t=1}^{n}\left(x_{s,t} - x_{0,t}\right)^2}{\sum_{t=1}^{n}\left(x_{0,t} - \mu_0\right)^2} = 1 - \frac{MSE}{\sigma_0^2} \tag{5}$$

Where n is the total number of time steps, $x_{s,t}$ is the simulated value at time t and μ_0 and σ_0 are the mean and standard deviation of the observed values.

The bias percentage assesses the average tendency of the simulated data to overestimate or underestimate the observed data. The *P* and *R* factors are uncertainty statistics about the 95PPU prediction interval, where the P-factor refers to the percentage of observed data falling within the 95PPU prediction band, and the R-factor indicates the width of the 95PPU prediction band (Abbaspour, 2015), which the narrower, the less uncertainty it indicates (Abbaspour, 2005).

From the initial best simulation and the sensitivity analyses, the software suggests a series of meaningful parameters to perform the calibration (Table 3). In each of the study sub-basins, flow calibration was carried out for each of the six scenarios, with a variable number between four and eight parameters (Table 4 and Table 5), depending on the sensitivity of each simulation to variations in the parameters involved.

Table 3. Parameters used in the discharge calibration of the three sub-basins.

	Acronym	Description of the parameter	Hydrologycal component
1	R_CN2.mgt	SCS runoff curve number for moisture condition II	Surface runoff
2	V_ALPHA_BF.gw	Base flow alpha factor ($days^{-1}$)	Groundwater
3	V_GW_DELAY.gw	Groundwater delay (days)	
4	V_GWQMN.gw	Threshold water level in shallow aquifer for base flow (mm H_2O)	
5	R_SOL_AWC(..).sol	Soil available water storage capacity (mm H_2O/mm soil)	Soil water
6	R_ESCO.hru	Soil evaporation compensation factor at HRU level	Potential and real evapotranspiration
7	R_ESCO.bsn	Soil evaporation compensation factor at basin level	
8	V_GW_REVAP.gw	Groundwater revaporization coefficient	
9	V_REVAPMN.gw	Threshold depth of water in shallow aquifer for revaporization to occur (mm H_2O)	

Table 4. Initial and final ranges of the parameters used in the flow calibration and efficiency statistics of the TES basin for each of the modeled periods.

No.	Acronym	Initial range (min/max)					
		Period					
		1985-1986	1987-1993	1994-1998	1999-2003	2004-2011	2012-2018
1	R_CN2.mgt	-0.1/ 0.11	-0.16/ -0.12	-0.2/ -0.07	-0.2/ -0.12	-0.2/ -0.15	-0.2/ -0.18
2	V_ALPHA_BF.gw	0.23/ 0.36	0.26/ 0.35	-0.01/ 0.95	-0.01/ 1.02	-0.05/ 0.2	0.29/ 0.4
3	V_GW_DELAY.gw	98.03/ 192.86	58.75/ 95.52	-3.08/ 262.89	277.78/ 541.58	20.21/ 152.76	123.94/ 203.7
4	V_GWQMN.gw	1.95/ 2.42	111.32/ 178.11	-1.38/ 0.34	-9.17/ 144.7	1.15/ 2.11	0.53/ 1.2
5	R_SOL_AWC(..).sol	-0.34/ 0.72	0/ 0.06	-0.34/ -0.14	0/ 0.77	0.02/ 0.48	-0.88/ -0.41
6	R_ESCO.hru	-0.12/ 0.51					
7	R_ESCO.bsn		0.31/ 0.72	-0.41/ -0.14	0.27/ 1.61	0.63/ 0.94	-0.02/ 0.26

See Table 3 for the description of the parameter represented by the acronym.

Tecnología y Ciencias del Agua

OPEN ACCESS

Check for updates

Table 5. Initial and final ranges of the parameters used in the flow calibration and efficiency statistics of the SJN basin for each of the modeled periods.

No.	Acronym	Initial range (min/max)					
		Period					
		1985-1986	1987-1993	1994-1998	1999-2003	2004-2011	2012-2018
1	R_CN2.mgt	-0.09/ 0.15	-0.09/ 0	-0.2/ 0.05	-0.2/ 0.06	-0.19/ -0.16	-0.2/ 0.04
2	V_ALPHA_BF.gw	0.32/ 1.03	0.02/ 0.39	-0.11/ 0.66	-0.4/ 0.55	0.39/ 0.61	0.45/ 1.4
3	V_GW_DELAY.gw	207.91/ 587.09	-8.05/ 122.06	-139.63/ 262.63	49.77/ 325.23	290.53/ 355.01	-107.24/ 272.24
4	V_GWQMN.gw	0.1/ 1.4	1.48/ 2.15	0.94/ 2.96	44.59/ 140.41	121.19/ 156.32	-0.65/ 1.15
5	R_SOL_AWC(..).sol				-0.57/ 0.33	0.51/ 0.66	0.08/ 0.71
6	R_ESCO.bsn				-1.3/ -0.45	0.45/ 0.67	0.25/ 0.8
7	V_GW_REVAP.gw					0.16/ 0.21	
8	V_REVAPMN.gw					17.94/ 159.06	

See Table 3 for the description of the parameter represented by the acronym.

Results

Land use change

The area of the TES sub-basin covered by temperate forests increased from 16 % in 1986 to 26 % in 2003 and then declined again in 2018 (Figure 2, graph of TES areas). For their part, the rain forests showed a 50 % loss in their extension from 1986 to 2018, with a marked decline in 2003 and, later, a recovery in the following 15 years. The areas occupied by chaparrals and rosetophyllous scrubs were less than 0.25 % in all scenarios.

Variations in natural plant cover are directly related to variations in production practices. The recovery of temperate forests was mainly due to the discontinuation of rainfed agriculture in the highlands between 1986 and 2003, while the decline in the period from 2003 to 2018 indicates human practices that promote deforestation. In turn, the decreased extension of the tropical forest in the lower parts occurred due to the clearing carried out for the expansion of pasture areas (for livestock purposes), which came to occupy half of the sub-basin in 2003. In subsequent years, the abandonment of the grasslands reduced their area to occupy only 30 % of the basin, allowing the recovery of secondary tropical forest vegetation in those places. From 1986 to 2003, the agricultural areas gradually reduced from 12 % to less than 1 % of the area. Later, in 2018, they expanded to occupy 20 % of the sub-basin.

The San Juan sub-basin is the southernmost one and has the lowest altitude (< 1 000 masl), so there are less areas covered with temperate forests (<5 %, except in 2003 and 2011) than in TES (Figure 2, graph of SJN areas). On the contrary, tropical forests covered 55 % of the area in 1993, followed by a degradation process that reduced it to a quarter in 2003 and a recovery phase in the last two decades. In all scenarios, chaparrals represented less than 0.05 % of the area (>400 ha).

Similarly to TES, the area lost to forests and tropical forests from 1986 to 2003 was gained by grasslands, which by 2003 had covered 68 % of the sub-basin and was later reduced to 39 %. As for agricultural areas, they have increased the occupied area from 10 % in 1986 to 25 % in 2018, with the lowest point reached in 2003. However, as discussed below in relation to the quality of the input data (see section The sources of uncertainty and the scope of modeling), the drastic changes registered in 2003 with respect to the previous (1998) and subsequent (2011) scenarios suggest the need to verify the results obtained for that year with a different set of images.

Tecnología y Ciencias del Agua

OPEN ACCESS

Check for updates

Hydrological modeling

The results presented in this section and the next are the product of the parameterization of the models with the best fit obtained according to the efficiency statistics. Table 4 (TES) and Table 5 (SJN) show the initial uncertainty ranges given by default by the model in reference, to which the final values of each parameter for each sub-basin were adjusted.

The graphs with the parameterized flow data with the best fit and the prediction intervals for each period are presented in Figure 4 and Figure 5, together with the respective efficiency and uncertainty statistics.

Tecnología y Ciencias del Agua

OPEN ACCESS

Check for updates

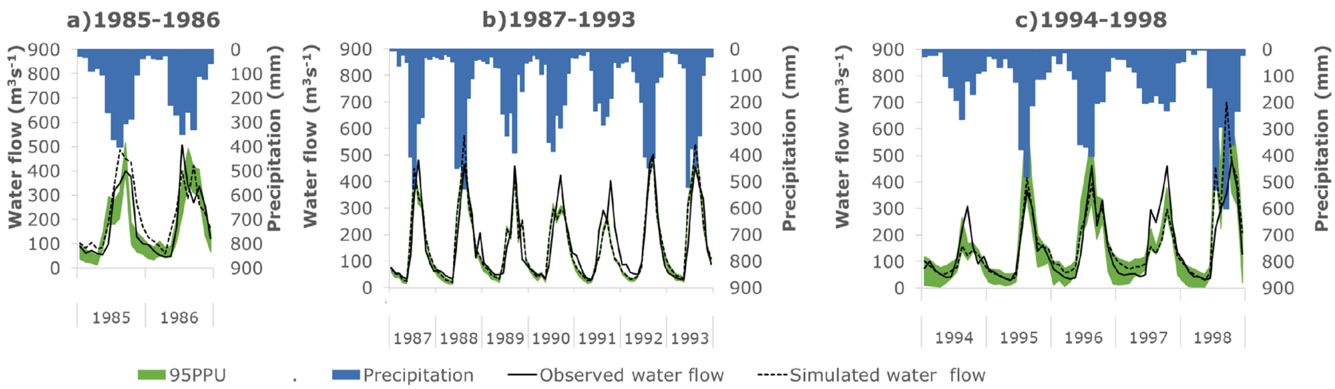

KGE	NSE	R²	PBIAS	P-factor	R-factor	KGE	NSE	R²	PBIAS	P-factor	R-factor	KGE	NSE	R²	PBIAS	P-factor	R-factor
0.85	0.66	0.68	-1.2	0.63	0.60	0.90	0.81	0.82	2.0	0.40	0.16	0.82	0.64	0.69	-3.3	0.77	0.57

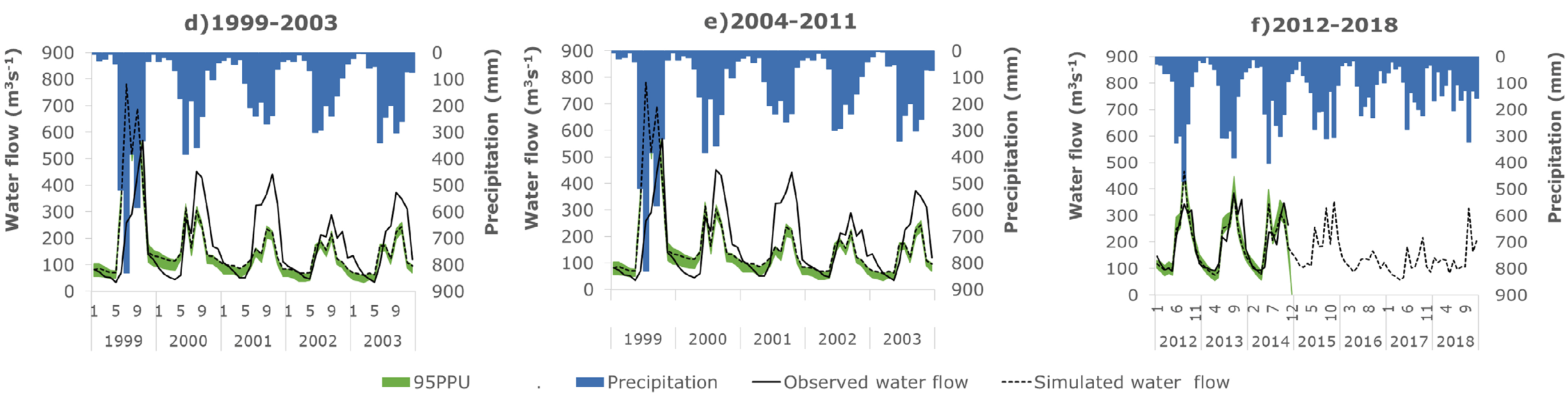

KGE	NSE	R²	PBIAS	P-factor	R-factor	KGE	NSE	R²	PBIAS	P-factor	R-factor	KGE	NSE	R²	PBIAS	P-factor	R-factor
0.58	0.14	0.35	7.50	0.28	0.24	0.89	0.78	0.60	0.8	0.73	0.85	0.85	0.70	0.74	2.20	0.77	0.52

Figure 1. Flow modeling for 1986–2014 (calibrated) and 2015–2018 (simulated) at the "Garro" hydrometric station of the Tesechoacán (TES) sub-basin. Each graph (section) corresponds to a modeled period (see Table 2).

Tecnología y Ciencias del Agua

OPEN ACCESS

Check for updates

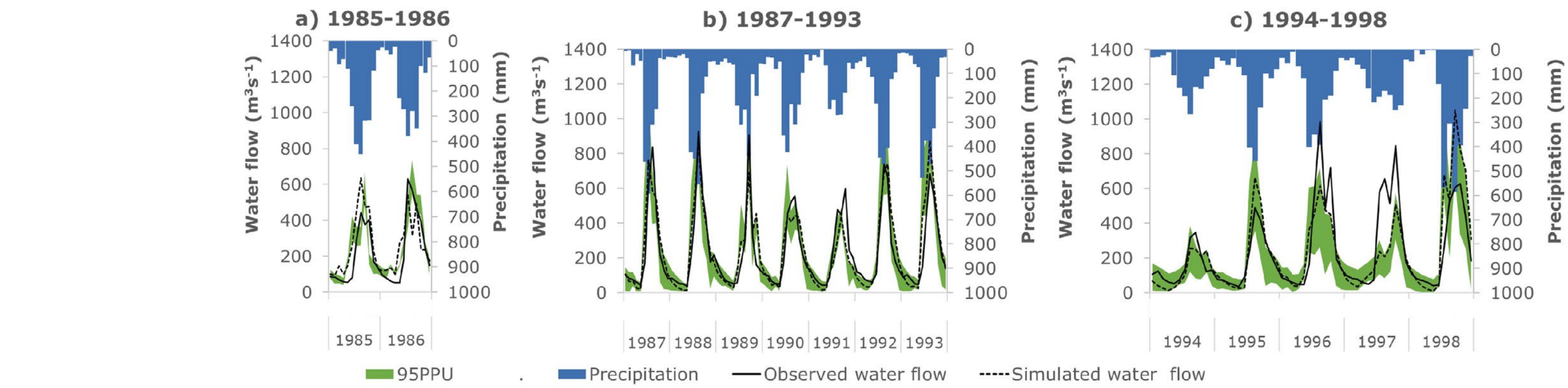

KGE	NSE	R²	PBIAS	P-factor	R-factor	KGE	NSE	R²	PBIAS	P-factor	R-factor	KGE	NSE	R²	PBIAS	P-factor	R-factor
0.79	0.62	0.65	-8.3	0.54	0.43	0.90	0.81	0.83	-2.7	0.82	0.72	0.78	0.57	0.62	3.40	0.72	0.65

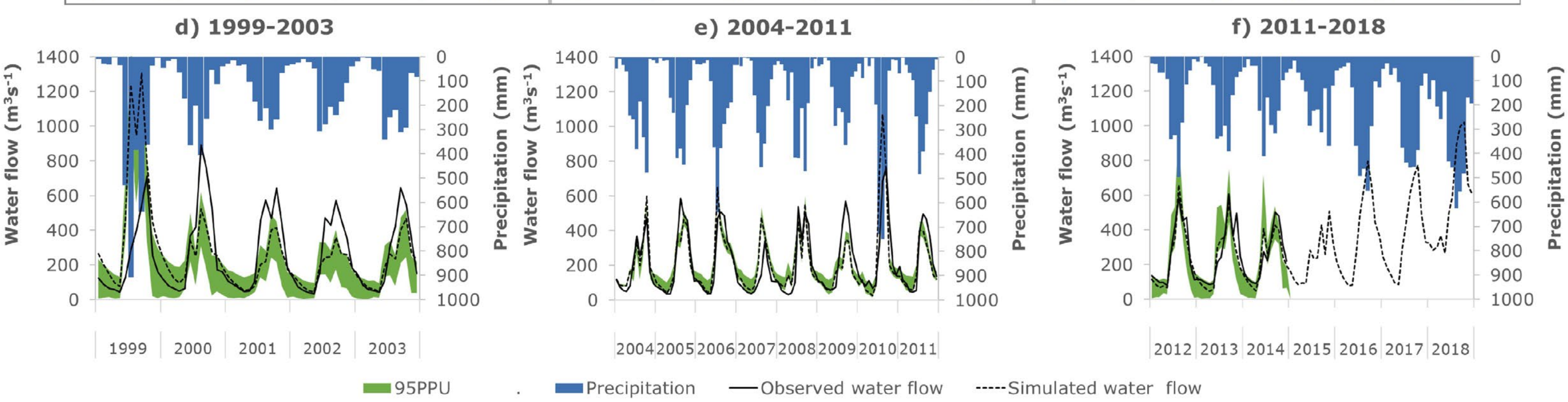

KGE	NSE	R²	PBIAS	P-factor	R-factor	KGE	NSE	R²	PBIAS	P-factor	R-factor	KGE	NSE	R²	PBIAS	P-factor	R-factor
0.54	-0.02	0.32	-3.50	0.52	0.42	0.84	0.67	0.70	1.0	0.57	0.39	0.89	0.83	0.85	6.7	0.75	0.76

Figure 2. Flow modeling for 1986–2014 (calibrated) and 2015–2018 (simulated) at the "Cuatotolapan" hydrometric station of the San Juan (SJN) sub-basin. Each graph (section) corresponds to a modeled period (see Table 2).

Regardless of the changes in vegetation and land use between the different scenarios by sub-basin, the same six parameters presented the best fit in TES (Table 4).

The bias percentage indicates that the results are good when they are in the range of ±15 % according to Moriasi *et al*. (2007). Abbaspour (2015) suggests that, in discharge calibration, P-factor values >70 % are considered optimal. The same author points out that the R-factor value must be less than 1.5, and for this sub-basin all the periods presented values between 0.31 and 0.58.

TES presents efficiency values in all the calibrated periods between 0.64 and 0.90, except in the 1999-2003 period (KGE = 0.58, NSE = 0.14, R^2 = 0.35) (Figure 4). The poor performance of the 1999–2003 period is verified in the low P-factor value = 0.28, the comparatively high bias coefficient (PBIAS = 7.5), as well as visually (Figure 4d). The uncertainty statistics confirm the satisfactory adjustment in the 1994–1998, 2004–2011 and 2012–2018 periods (values of P-factor greater than 70 % in the three cases) and indicate that the 1985–1986 period is slightly below the performance threshold (P-factor = 0.63). The first and third periods are slightly overestimated, while the rest of the periods present a slight underestimation. Although the period of the simulated data from 1987 to 1993 presented the best values of KGE, NSE and R^2 (> 0.80), only 40 % of the data observed in 1987–1993 coincide with the 95PPU interval (Figure 4b).

In SJN, surface runoff and groundwater, with one (R_CN2.mgt) and three (V_ALPHA_BF.gw, V_GW_DELAY.gw, V_GWQMN.gw) parameters, respectively, explained the behavior of water yield from 1986 to 1998, while from 2003 to 2018, soil water (R_SOL_AWC(..).sol) and potential and real evapotranspiration had greater relevance (Table 5).

Similarly to TES, in SJN (Figure 5), the 1999–2003 period shows the lowest efficiency values (< 0.54). In contrast, periods 1987–1993, 1994–1998, and 2012–2018 showed the best performance values in the KGE (0.90, 0.78, and 0.89, respectively), NSE (0.81, 0.57, and 0.83, respectively), and R^2 (0.83, 0.62, and 0.85, respectively) statistics, as well as in the P-factor (0.82, 0.72, and 0.75, respectively) and R-factor (0.72, 0.72, and 0.75, respectively). Although the 1985–1986 and 2004–2011 periods show good adjustments, the P-factor indicates a higher level of error with values of 0.54 and 0.57, respectively.

Modeling potential erosion

The potential erosion values estimated in this section correspond to the multi-annual averages of the six modeled flow periods. The average water erosion per scenario per sub-basin oscillates in the range of 69 to 158 ton ha^{-1} $year^{-1}$ in the Tesechoacán sub-basin and between 57 y 162 ton ha^{-1}

year^{-1} in San Juan (Table 6). According to these figures, the volume eroded in Tesechoacán has decreased to 44 % of the volume estimated in 1986, and in San Juan to 38 % of the initial estimate.

Table 6. Multi-annual average water erosion (ton ha^{-1} year^{-1}) per period per sub-basin.

Sub-basin	**Multi-annual average water erosion (ton ha^{-1} year^{-1})**					
	Period					
	1985-1986	1987-1993	1994-1998	1999-2003	2004-2011	2012-2018
Tesechoacán	158.4	73.83	108.36	81.1	80.46	69.17
San Juan	162.28	67.17	73.86	100.42	56.77	61.98

Figure 6 shows the spatial distribution of the erosive potential of HRUs by sub-basin, classified into four erosion categories: none to light, moderate, high, and very high (FAO, 1980). In TES, the greatest erosion, especially notable in 1986, occurred in the upper part of the sub-basin, where temperate forests are concentrated on steep slopes, followed by the middle basin, with moderate to high erosion, while the lower part reported light to moderate volumes in all scenarios. In the SJN sub-basin, on the other hand, the areas of greatest erosion are also located in the areas of highest elevation, although, during the different periods, small areas with very high erosion are observed in the middle and low areas. In this sub-basin, a reduction in the area affected by more severe levels of water erosion is observed.

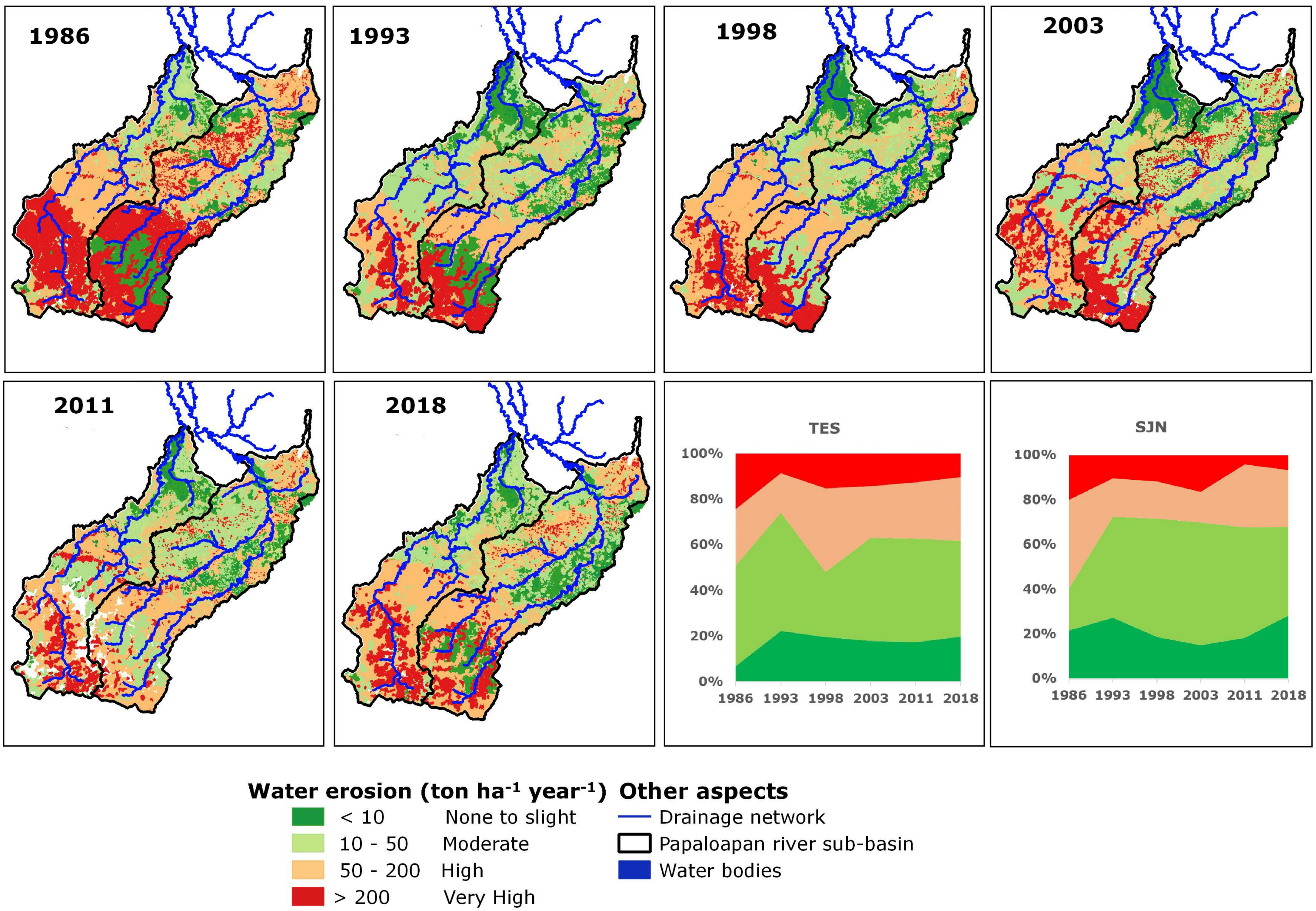

Figure 3. Distribution of the erosive potential by sub-basin according to FAO's classification (FAO, 1980).

In percentage terms (Figure 6, graph of TES areas), more than 50 % of the TES basin shows moderate erosion during all the scenarios, except in 1986 and 1998, when the area with high erosion increased. Areas with light and very high erosion represented each less than 20 % of each scenario, on average. In the SJN sub-basin (Figure 6, graph of SJN areas), between 40 % and 55 % of the area reported erosion levels between 10-50 ton ha^{-1} $year^{-1}$, except in 1986; all other levels remained mostly below 20 %.

Discussion

Precipitation variability and observed flows

For the 1986–2018 period, the average rainfall was 1,795 mm in TES and 2,250 mm in SJN. Both sub-basins registered the lowest levels of precipitation in the 1994-1998 period, with up to 450 mm less (in SJN) than the above-mentioned average, coinciding with one of the periods (1997–1998), in which the El Niño–Southern Oscillation (ENSO) meteorological phenomenon had a greater impact on the national territory

(Escobar-Briones, Bonilla, Badán, Caballero, & Winckell, 2001). This decrease was observed in reductions of between 5 and 10 % of the average flow for the 1994-1998 period in the two sub-basins, with respect to the other periods. In contrast, precipitation for the 2012-2018 period in SJN exceeded more than 50 % the average of the 34 years analyzed, with atypical monthly maximum values above 500 mm in the rainy seasons of 2017 and 2018 (Conagua, 2018).

The average flow observed for the six study periods ranged between 151 and 196 $m^3 s^{-1}$ in TES and between 208 and 251 $m^3 s^{-1}$ in SJN. This variability in each basin is explained on two time scales. First, the seasonality of the annual precipitation is reflected in the amplitude of the monthly ranges of the values of flows observed and simulated for each period evaluated by sub-basin (Figure 4 and Figure 5). Second, the influence of ENSO is responsible for reductions of about 10 % in summer rainfall and increases of about 20 % in winter rainfall in the years 1986–1987, 1991–1992, 1994, 1997–1998, and 2002 (Magaña, Pérez, & Conde, 1998; Magaña, Vázquez, Pérez, & Pérez, 2003).

Land use change and sediment production

From 1986 to 1993, TES and SJN showed a reduction of more than 50 % in the volume of erosion produced (Table 6), attributable to the increase in forest and rainforest cover (Figure 2).

In the 1998 period, an increase was observed in the area with the greatest severity of erosion —from moderate (10 ton ha^{-1} $year^{-1}$) to high (10-50 ton ha^{-1} $year^{-1}$)— in the middle zone of the TES sub-basin (Figure 6). This exacerbation is mainly related to the expansion of grasslands, which, although they continued to expand until 2003 (Figure 2), no longer reflected the increase in average erosion of that period. In contrast, in the 2003 scenario, a decrease in the area affected by high erosion and a 25 % lower sediment production is observed in TES compared to the previous period (Table 6). This decrease is possibly associated with the reduction of agricultural land use in favor of forest recovery, particularly in the upper basin, similar to what was found by Muñoz-Villers and López-Blanco (2008) in La Antigua, a basin of the same hydrological region, in the same period. However, the 2003 vegetation and land use scenario presented the most drastic changes in primary vegetation in favor of grasslands (Figure 2). In SJN, the expansion of grasslands is also marked, especially in the tropical forests, and this change translated into an increase in erosion in 2003 of around 35 % compared to the previous period (Table 6).

In the period from 2004 to 2018, TES and SJN showed lower volumes of erosion, possibly related to the typical rapid recovery of tropical vegetation in the upper and middle areas (Figure 4), but the agricultural area also expands in the form of patches along the two sub-basins (Figure 2).

Cycles of substitution of primary vegetation by areas of agricultural and/or livestock use are observed, which may be temporarily abandoned to natural regeneration and later reopened for grazing or agriculture (Alavez-Vargas *et al*., 2021).

In this study, it has been possible to relate the changes in sediment production with the cover only when the vegetation cover is modified in extensive areas of low slope, such as the increase of grasslands in the low areas or when it happens in the steep areas of basin headwaters, such as deforestation for agricultural use. A study in the La Antigua basin effectively documented a greater production of sediments in grasslands compared to forest areas (Martínez *et al*., 2009).

In these case studies, it was found that the topography of the Papaloapan is dominated by areas with slopes lower than 15 %, so that, while the headwaters can reach steep slopes of more than 2,000 masl, more than half of the landscape of each sub-basin consists of wide alluvial plains that work as sediment deposit areas (Verstraeten *et al*., 2009; Wohl *et al*., 2012). In other words, regardless of their source, the sediments produced are not exported outside the sub-basin, since no statistically significant trends were observed in the volume of sediments transported by the river between 1986 and 1998 (Alavez-Vargas *et al*., 2021). Similarly, the meta-analysis carried out by Guzha *et al*. (2018) in the African tropics revealed low correlations between forest cover and runoff, thus emphasizing the need to improve long-term basin monitoring programs to increase the understanding of hydrological responses.

Potential erosion and historical data scarcity

The annual production of sediments estimated with MUSLE uses runoff as the energy factor of particle detachment and transport, instead of the erosivity factor of the precipitation of USLE (Williams & Berndt, 1977). For this reason, the availability of observed data for calibration is essential, since flow adjustment automatically implies an adjustment to the estimated erosion, and its omission can lead to significant under- or over-estimates.

The lack of historical records of erosion measurements was foreseen as a limitation to the scope of this study, since it would limit the validation of the estimates. Therefore, we proceeded as follows: for the last simulated period (2012–2018), we used the available soil erosion cartography of Mexico (INEGI, 2014), which was developed using different techniques for the analysis of satellite images, as well as information on soil profiles, which shows four categories of erosion based on the observed soil attributes (Bolaños-González *et al.*, 2016). Under the criteria of such information, most of the eroded areas in TES were classified as light and moderate, presenting a greater extension in the middle and lower zones, where their zones of "strong" erosion (bedrock exposure in 50–90 % of the erosion polygon) coincide with our high erosion results (50-200 ton ha^{-1} year^{-1}).

In SJN, moderate erosion polygons are concentrated in the high and low zones in the same areas that we classified as with very high erosion (> 200 ton ha^{-1} year^{-1}). This comparison is limited by the absence of volumetric units in the aforementioned cartography; however, the cartography of Borrelli *et al.* (2017), estimated at a spatial resolution of 250 m, identifies numerous points of water erosion greater than 20 ton ha^{-1} year $^{-1}$ in our study area. In contrast, the study conducted by Montes-León *et al.* (2011) classifies most of the Papaloapan basin (and therefore, the two sub-basins studied here) in erosion categories above 50 ton ha^{-1} year^{-1}.

The divergence between the estimates of the cited studies, together with the high level of erosion diagnosed in the country, referred to at the beginning of this document, ratifies the importance of having field information in order to make a better measurement not only of the current state of soils and vegetation cover of the basins, but also of the scope of the results of studies such as this one. Similarly, Tan *et al.* (2019) conclude from their meta-analysis in Southeast Asia that it is urgent to aim the efforts towards the in-field generation of good quality data, which are essential for modeling and prediction purposes.

The sources of uncertainty and the scope of modeling

The SWATCUP software was developed as a calibration tool for SWAT with the aim of systematizing, through five possible algorithms, the sensitivity and uncertainty analyzes and the parameterization involved in the calibration process, given the large number of parameters included in each SWAT modeling (Abbaspour, 2015).

In a comparison of SWATCUP calibration methods conducted on the Ganges River, Shivhare, Dikshit and Dwivedi (2018) documented a better performance of SUFI-2 over GLUE or ParaSol, supporting its widespread use (Abbaspour *et al.*, 2015; Arnold *et al.*, 2012; Chotpantarat & Boonkaewwan, 2018). In this research, the selection of the optimal group of parameters for calibration was made based on the initial recommendations of the calibration algorithm and the sensitivity analysis, as well as the guidance of previous studies (Abbaspour *et al*., 2015; Arnold *et al*., 2012). The optimal set of parameters for each modeling included: 1 for surface runoff, 3 for groundwater, 1 for soil water, and 1-3 for potential and actual evapotranspiration (Table 3, Table 4, and Table 5), which have been used for hydrological calibration in other recent studies both at a regional scale in Thailand (Chotpantarat & Boonkaewwan, 2018) and at a continental scale in Europe (Abbaspour *et al*., 2015) with good results. Tan *et al*. (2019) found good levels of SWAT performance in simulating flows in tropical regions from the analysis of 126 studies from Southeast Asia.

According to Moriasi *et al*. (Moriasi *et al*., 2007; Moriasi, Gitau, Pai, & Daggupati, 2015) the efficiency values of NSE>0.50 and PBIAS±15 %, can be considered satisfactory in the performance of monthly flow modelings. Under these criteria, the 12 study periods had fairly good percentages of bias (between -8.3 and 7.5), while according to the Nash-Sutcliffe efficiency criterion, 6 of 10 calibrated periods were satisfactory, the exception being the 1999–2003 period in the two sub-basins, as shown in Figure 4d and Figure 5d. The value of the Kling-Gupta objective function being close to 1 is just as important as the error of the models tending to 0, i.e., that the highest percentage of the observed data should be located in the narrowest prediction interval (95PPU) (R-factor→0) of the best parameterization (P-factor→1).

With this combination of criteria, the best simulations of this study simultaneously reached KGE and P-factor values greater than 0.70 and correspond to the calibrated periods of 1994–1998, 2004–2011, and 2012–2018 in TES (Figure 4c, 4d, and 4e) and 1987–1993, 1994–1998, and 2012–2018 in SJN (Figure 5b, 5c, and 5e). The performance of the 1986–1993 simulation in TES is observed in a lower range, with P-factor = 0.63 (Figure 4b), while the remaining simulations show errors greater than 40 %. As documented by Tan *et al*. (2019) studies carried out in tropical areas under conditions of data scarcity frequently omit the description of their error metrics, and these are important to carry out a more rigorous evaluation of the results, even if they show, as in this study, important anomalies that should be watched for in subsequent studies.

Abbaspour *et al*. (Abbaspour *et al*., 2007; Abbaspour *et al*., 2015) mention four sources of uncertainty in modeling: 1) conceptual simplification, 2) processes not simulated by the model, 3) processes simulated by the model, but unknown by the modeler or not modelable due to lack of data, and 4) the quality of input data. Points 3 and 4 were especially influential in this research.

Regarding the estimation of water erosion, it was decided to make the a priori assumption of the absence of conservation practices (factor PUSLE=1 of MUSLE) due to the lack of historical records. Regarding the quality of the data, the drastic change in vegetation of the 2003 scenario—compared to the previous one (1998) and the subsequent one (2011)—and the poor performance of the hydrological simulations of 1999–2003 in the two sub-basins suggest the need to reanalyze that scenario with a different set of images. Possibly, the irregularity of the intervals between the evaluated coverage and land use scenarios was a source of uncertainty for the model.

The capacity of the models to reconstruct trajectories of hydrological change has as its main limitation the existence (or not) of observed historical data to validate the generated scenarios; however, these continue to be useful tools to establish baselines (Arheimer & Lindström, 2019) and, in these cases, the comparison with estimates from other models can be used as a strategy for validating the results (Borrelli *et al*., 2017) and limiting the scopes.

Conclusions

The response of potential erosion in two medium-scale tropical hydrological sub-basins with respect to changes in land use was studied. To perform this quantification, the semi-distributed hydrological model Soil and Water Assessment Tool (SWAT) was used.

Of the 12 simulated periods, 2 were invalidated due to anomalies in the land use scenario. Based on the combined evaluation of three efficiency and two uncertainty statistic data sets, six of the ten remaining calibrated periods showed good fitting in the hydrological simulation with

KGE>0.70 and P-factor>0.70. According to the estimates made, a reduction in the volumes of water erosion was observed in the medium term.

The quality of the results was evaluated through the combined use of three efficiency statistics and two measurements of uncertainty. When using hydrological models for research and support for public policy decision-making, professionals and academicians are recommended to select a combination of statistics equivalent to the one used in this study, in order to verify jointly and with greater rigor the reliability of the modelings.

The comparison of the volumes of potential erosion estimated with respect to the results obtained by other studies in the same study area, albeit with different methods and scales, allows validating the results and limiting the scopes.

Likewise, the heterogeneity observed between the studies that were reviewed and the high level of erosion diagnosed in the country allows us to argue in favor of the need to generate standards and criteria for the production of good-quality data for the research and management of erosion in Mexico.

In countries like Mexico, with limited monitoring, the estimation of the variables of interest from physical, climate and human data, as well as the availability of resampling databases, has popularized the use of SWAT. The features of this tool are valuable for prospecting ungauged basins or chronosequences of interest; however, its applications for research or management purposes must be supported by error metrics as well as by efficiency statistics that clearly measure the scope, limitations and anomalies of the results.

Physically based models are useful tools in tropical regions with a scarce historical data to estimate the behavior of hydrological and edaphological dynamics, but given the levels of uncertainty found in this study, it is considered that they cannot permanently substitute the functions of a basin-scale erosion monitoring network.

Acknowledgements

This study was done as the first author was enrolled in the PhD Program of the Tropical Agricultural Research and Higher Education Center, with funds by the Mexican National Council for Science and Technology (Conacyt) and the project DGAPA-UNAM IA104918 from the Instituto de Ingeniería, Universidad Nacional Autónoma de México (II-UNAM).

References

Abbaspour, K. C. (2005). Calibration of hydrologic models: When is a model calibrated? In: Zerger, A., & Argent, R. M. (eds.). *MODSIM 2005 International Congress on Modelling and Simulation. Modelling and Simulation Society of Australia and New Zealand* (pp. 2449-12455). Melbourne, Australia.

Abbaspour, K. C., Johnson, C. A., & van Genuchten, M. T. (2004). Estimating uncertain flow and transport parameters using a sequential uncertainty fitting procedure. *Vadose Zone Journal*, 3(4), 1340-1352. Recovered from https://doi.org/10.2136/vzj2004.1340

Abbaspour, K. C., Vaghefi, S., & Srinivasan, R. (2017). A guideline for successful calibration and uncertainty analysis for soil and water assessment: A review of papers from the 2016 International SWAT Conference. *Water*, 10(1), 6. Recovered from https://doi.org/10.3390/w10010006

Abbaspour, K. C., Rouholahnejad, E., Vaghefi, S., Srinivasan, R., Yang, H., & Kløve, B. (2015). A continental-scale hydrology and water quality model for Europe: Calibration and uncertainty of a high-resolution large-scale SWAT model. *Journal of Hydrology*, 524, 733-752. Recovered from https://doi.org/10.1016/J.JHYDROL.2015.03.027

Abbaspour, K. C. (2015). *SWAT-CUP: SWAT calibration and uncertainty programs. A user manual* (100 p.). Dübendorf, Switzerland: Swiss Federal Institute of Aquatic Science and Technology, Eawag.

Abbaspour, K. C., Yang, J., Maximov, I., Siber, R., Bogner, K., Mieleitner, J., Zobrist, J., & Srinivasan, R. (2007). Modelling hydrology and water quality in the pre-alpine/alpine Thur watershed using SWAT. *Journal of Hydrology*, 333(2-4), 413-430. Recovered from https://doi.org/10.1016/J.JHYDROL.2006.09.014

Alatorre, L. C., & Beguería, S. (2009). Los modelos de erosión: una revisión. *Revista C&G*, 23(1-2), 29-48.

Alavez-Vargas, M., Birkel, C., Corona, A., & Breña-Naranjo, J. A. (2021). Land cover change induced sediment transport behaviour in a large tropical Mexican catchment. *Hydrological Sciences Journal*, 66(6), 1069-1082. Recovered from https://doi.org/10.1080/02626667.2021.1903472

Arheimer, B., & Lindström, G. (2019). Detecting changes in river flow caused by wildfires, storms, urbanization, regulation and climate across Sweden. *Water Resources Research*, 55(11), 8990-9005. Recovered from https://doi.org/10.1029/2019wr024759

Arnold, J. G., Kiniry, J. R., Srinivasan, R., Williams, J. R., Haney, E. B., & Neitsch, S. L. (2011). *Soil and water assessment tool. Input/output file documentation* (Issue December). San Antonio, USA: Texas A&M University System.

Arnold, J. G., Moriasi, D. N., Gassman, P. W., Abbaspour, K. C., White, M. J., Srinivasan, R., Santhi, C., Harmel, R. D., Griensven, A. van, Liew, M. W., Kannan, N., & Jha, M. K. (2012). SWAT: model use, calibration and validation. *Transactions of the ASABE*, 55(4), 1491-1508.

Beaudoing, H., & Rodell, M. (2015). *GLDAS Noah Land Surface Model L4 3 hourly 0.25 x 0.25 degree V2.0*. GES DISC. Recovered from https://doi.org/10.5067/342OHQM9AK6Q

Beaudoing, H., & Rodell, M. (2016). *GLDAS Noah Land Surface Model L4 3 hourly 0.25 x 0.25 degree V2.1*. Greenbelt, Maryland, USA, Goddard Earth Sciences Data and Information Services Center (GES DISC), Recovered from https://disc.gsfc.nasa.gov/datasets/GLDAS_NOAH025_3H_2.1/summary

Bello, J., Gómez, L., Magaña, V., Graizbord, B., & Rodríguez, P. H. (2009). Sitio piloto río Papaloapan-Laguna de Alvarado. En: Buenfil-Friedman, J. (ed.). *Adaptación a los impactos del cambio climático en los humedales costeros del Golfo de México.* (pp. 435-456). México, DF, México: Secretaría del Medio Ambiente y Recursos Naturales, e Instituto Nacional de Ecología.

Beven, K. (2012). *Rainfall-runoff modelling: the primer*. Noida, India: Wiley-Blackwell.

Blackman, A., Goff, L., & Rivera-Planter, M. (2018). Does eco-certification stem tropical deforestation? Forest Stewardship Council certification in Mexico. *Journal of Environmental Economics and Management*, 89(C), 306-333. Recovered from https://doi.org/10.1016/j.jeem.2018.04.005

Bolaños-González, M. A., Paz-Pellat, F., Cruz-Gaistardo, C. O., Argumedo-Espinoza, J. A., Romero-Benítez, V. M., & De-la-Cruz-Cabrera, J. C. (2016). Mapa de erosión de los suelos de México y posibles implicaciones en el almacenamiento de carbono orgánico del suelo. *TERRA Latinoamericana*, 34(3), 271-288.

Borrelli, P., Robinson, D. A., Fleischer, L. R., Lugato, E., Ballabio, C., Alewell, C., Meusburger, K., Modugno, S., Schütt, B., Ferro, V., Bagarello, V., Oost, K. Van, Montanarella, L., & Panagos, P. (2017). An assessment of the global impact of 21st century land use change on soil erosion. *Nature Communications*, 8(1), 2013. Recovered from https://doi.org/10.1038/s41467-017-02142-7

Cardoza-Vázquez, R., Cuevas-Flores, L., García-Carreón, J. S., Guerrero-Herrera, J. A., Gonzalez-Olarte, J. C., Hernández-Méndez, H., Lira-Quintero, M. de L., Nieves-Frausto, J. L., Tejeda-Sartorius, D., & Vázquez-Martinez, C. M. (2007). *Protección, restauración y conservación de suelos forestales. Manual de obras y prácticas*. Comisión Nacional Forestal, y Secretaría del Medio Ambiente y Recursos Naturales.

Carvalho, L. M. V. (2019). Assessing precipitation trends in the Americas with historical data: A review. *Wiley Interdisciplinary Reviews: Climate Change*, e627. Recovered from https://doi.org/10.1002/wcc.627

Chotpantarat, S., & Boonkaewwan, S. (2018). Impacts of land-use changes on watershed discharge and water quality in a large intensive agricultural area in Thailand. *Hydrological Sciences Journal*, 63(9), 1386-1407. Recovered from https://doi.org/10.1080/02626667.2018.1506128

Conagua, Comisión Nacionald el Agua. (2017). *Banco Nacional de Datos de Aguas Superficiales (BANDAS)*. Recovered from https://www.imta.gob.mx/bandas

Conagua, Comisión Nacionald el Agua. (octubre, 2018). *Reporte del clima en México*, 8(10), 43.

Couto, A. A., Da-Conceição, F. T., Fernandes, A. M., Spatti, E. P., Lupinacci, C. M., & Moruzzi, R. B. (2019). Land use changes associated with the expansion of sugar cane crops and their influences on soil removal in a tropical watershed in São Paulo State (Brazil). *Catena*, 172 (December 2017), 313-323. Recovered from https://doi.org/10.1016/j.catena.2018.09.001

Delmas, M., Cerdan, O., Cheviron, B., & Mouchel, J. M. (2011). River basin sediment flux assessments. *Hydrological Processes*, 25(10), 1587-1596. Recovered from https://doi.org/10.1002/hyp.7920

Dile, Y., Srinivasan, R., & George, C. (2019). *QGIS Interface for SWAT (QSWAT) version 1.8* (p. 98). Recovered from https://swat.tamu.edu/media/116371/qswat-manual_v19.pdf

Douglas-Mankin, K. R., Srinivasan, R., & Arnold, J. G. (2010). Soil and Water Assessment Tool (SWAT) model: Current developments and applications. *Transactions of the ASABE*, 53(5), 1423-1431.

Escobar-Briones, E., Bonilla, M., Badán, A., Caballero, Ma., & Winckell, A. (2001). *Los efectos del fenómeno El Niño en México 1997-1998*. México, DF, México: Consejo Nacional de Ciencia y Tecnología.

Fakhri, M., Dkohaki, H., Eslamian, S., Fazeli-Farzani, I., & Reza-Farzaneh, M. (2014). Flow and sediment transport modeling in rivers. In: Eslamian, S. (ed.). *Handbook of engineering hydrology. Modeling, climate change and variability* (pp. 233-275). Boca Raton, USA: CRC Press.

FAO, Organización de las Naciones Unidas para la Alimentación y la Agricultura. (1980). *Metodología provisional para la evaluación de la degradación de los suelos.* Roma, Italia: Organización de las Naciones Unidas para la Alimentación y la Agricultura.

FAO, Organización de las Naciones Unidas para la Alimentación y la Agricultura. (2009). *Guía para la descripción de suelos*. Roma, Italia: Organización de las Naciones Unidas para la Alimentación y la Agricultura.

FAO, Organización de las Naciones Unidas para la Alimentación y la Agricultura. (2011). *Situación de los bosques del mundo*. Roma, Italia: Organización de las Naciones Unidas para la Alimentación y la Agricultura.

FAO & ITPS, Organización de las Naciones Unidas para la Alimentación y la Agricultura & Intergovernmental Technical Panel on Soils (ITPS). (2015). *The status of the world's soil resources. Main report*. Recovered from https://www.fao.org/3/i5199e/i5199e.pdf

García, E. (2004). *Modificaciones al sistema de clasificación climática de Köppen* (5th ed.). México, DF, México: Instituto de Geografía- Universidad Nacional Autónoma de México.

Goodchild, M. F. (1996). *Environmental modelling with GIS*. Oxford , UK: Oxford University Press.

Gupta, H. V., Kling, H., Yilmaz, K. K., & Martínez, G. F. (2009). Decomposition of the mean squared error and NSE performance criteria: Implications for improving hydrological modelling. *Journal of Hydrology*, *377*(1-2), 80-91. Recovered from https://doi.org/10.1016/j.jhydrol.2009.08.003

Guzha, A. C., Rufino, M. C., Okoth, S., Jacobs, S., & Nóbrega, R. L. B. (2018). Impacts of land use and land cover change on surface runoff, discharge and low flows: Evidence from East Africa. *Journal of Hydrology: Regional Studies*, 15(November 2017), 49-67. Recovered from https://doi.org/10.1016/j.ejrh.2017.11.005

Hargreaves, G. L., Hargreaves, G. H., & Riley, J. P. (1985). Agricultural benefits for Senegal river basin. *Journal of Irrigation and Drainage Engineering*, 111(2), 113-124. Recovered from https://doi.org/10.1061/(ASCE)0733-9437(1985)111:2(113)

INEGI, Instituto Nacional de Estadística y Geografía. (2007). *Conjunto de datos vectorial edafológico escala 1:250000 serie II (Continuo Nacional)*. INEGI.

INEGI, Instituto Nacional de Estadística y Geografía. (2010). *Red hidrográfica escala 1:50 000*. Aguascalientes, México: Instituto Nacional de Estadística y Geografía.

INEGI, Instituto Nacional de Estadística y Geografía. (2013). *Conjunto de datos de perfiles de suelo escala 1:250000 serie II (Continuo Nacional)*. Aguascalientes, México: Instituto Nacional de Estadística y Geografía.

INEGI, Instituto Nacional de Estadística y Geografía. (2014). *Carta de erosión de suelo. Escala 1: 250 000. Serie I*. Aguascalientes, México: Instituto Nacional de Estadística y Geografía.

Jajarmizadeh, M., Harun, S., & Salarpour, M. (2012). A review on theoretical consideration and types of models in Hydrology. *Journal of Environmental Science and Technology*, 5(5), 249-261. Recovered from https://doi.org/10.3923/jest.2012.249.261

Jarvis, A., Reuter, H. I., Nelson, A., & Guevara, E. (2008). *Hole-filled SRTM for the globe Version 4: data grid, CGIAR-CSI SRTM 90m Database*. CGIAR Consortium for Spatial Information. Recovered from http://srtm.csi.cgiar.org/

Jørgensen, S. E., & Fath, B. D. (2011). *Fundamentals of ecological modelling: Applications in environmental management and research* (4th ed.). USA: Elsevier. Recovered from https://www.amazon.com/Fundamentals-Ecological-Modelling-Applications-Environmental/dp/0444535675?asin=0444535675&revisionId=&format=4&depth=1

Li, B., Beaudoing, H., & Rodell, M. (2018). *GLDAS catchment land surface model L4 daily 0.25 x 0.25 degree V2.0*. GES DISC. Recovered from https://doi.org/10.5067/LYHA9088MFWQ

Liu, J., Zhang, C., Kou, L., & Zhou, Q. (2017). Effects of climate and land use changes on water resources in the Taoer River. *Advances in Meteorology*, 2017, 1-13. Recovered from https://doi.org/10.1155/2017/1031854

Magaña, V., Pérez, J., & Conde, C. (1998). El fenómeno del El Niño y la oscilación del sur. Sus impactos en México. *Ciencias*, 51, 14-18.

Magaña, V. O., Vázquez, J. L., Pérez, J. L., & Pérez, J. B. (2003). Impact of El Niño on precipitation in Mexico. *Geofísica Internacional*, 42(3), 313-330.

Martinez, J. M., Guyot, J. L., Filizola, N., & Sondag, F. (2009). Increase in suspended sediment discharge of the Amazon River assessed by monitoring network and satellite data. *Catena*, 79(3), 257-264. Recovered from https://doi.org/10.1016/j.catena.2009.05.011

Martínez, M. L., Pérez-Maqueo, O., Vázquez, G., Castillo-Campos, G., García-Franco, J., Mehltreter, K., Equihua, M., & Landgrave, R. (2009). Effects of land use change on biodiversity and ecosystem services in tropical montane cloud forests of Mexico. *Forest Ecology and Management*, 258(9), 1856-1863. Recovered from https://doi.org/10.1016/j.foreco.2009.02.023

Montes-León, M. A. L., Uribe-Alcántara, E. M., & García-Celis, E. (2011). Mapa nacional de erosión potencial. *Tecnología y ciencias del agua*, 2(1), 5-17.

Moriasi, D. N., Arnold, J. G., Van Liew, M. W., Bingner, R. L., Harmel, R. D., & Veith, T. L. (2007). Model evaluation guidelines for systematic quantification of accuracy in watershed simulations. *Transactions of the ASABE*, 50(3), 885-900. Recovered from https://doi.org/10.13031/2013.23153

Moriasi, D. N., Gitau, M. W., Pai, N., & Daggupati, P. (2015). Hydrologic and water quality models: Performance measures and evaluation criteria. *Transactions of the ASABE*, 58(6), 1763-1785.

Muñoz-Villers, L. E., & López-Blanco, J. (2008). Land use/cover changes using Landsat TM/ETM images in a tropical and biodiverse mountainous area of central-eastern Mexico. *International Journal of Remote Sensing*, 29(1), 71-93. Recovered from https://doi.org/10.1080/01431160701280967

Neitsch, S., Arnold, J., Kiniry, J., & Williams, J. (2011). *Soil & water assessment tool theoretical documentation version 2009*. Texas Water Resources Institute. Recovered from https://doi.org/10.1016/j.scitotenv.2015.11.063

Pérez-Vega, A., & Ortiz-Pérez, M. (2002). Cambio de la cubierta vegetal y vulnerabilidad a la inundación en el curso bajo del río Papaloapan, Veracruz. *Investigaciones Geográficas*, 48, 90-105.

QGIS Development Team. (2014). *QGIS Geographic Information System v. 2.6.1. Brighton. Open Source*. Recovered from https://download.qgis.org/downloads/

QGIS Development Team. (2019). *QGIS Geographic Information System. Open Source*. Geospatial Foundation Project. Recovered from http://qgis.osgeo.org

Rangel, L., Jorge, M. do C., Guerra, A., & Fullen, M. (2019). Soil erosion and land degradation on trail systems in mountainous areas: Two case studies from South-East Brazil. *Soil Systems*, 3(3), 56. Recovered from https://doi.org/10.3390/soilsystems3030056

Reid, L. M. (1998). Cumulative watershed effects and watershed analysis. In: Naiman, R. J., & Bilby, R. E. (eds.). *River ecology and management: Lessons from the Pacific Coastal Ecoregion* (pp. 476-501). Tacoma, USA: Springer-Verlag.

Rodell, M., Houser, P. R., Jambor, U., Gottschalck, J., Mitchell, K., Meng, C.-J., Arsenault, K., Cosgrove, B., Radakovich, J., Bosilovich, M., Entin, J. K., Walker, J. P., Lohmann, D., & Toll, D. (2004). The global land data assimilation system. *Bulletin of the American Meteorological Society*, 85(3), 81-394.

Ruiz-Fernández, A. C., Maanan, M., Sanchez-Cabeza, J. A., Bernal, L. H. P., Mendoza, P. L., & Limoges, A. (2014). Chronology of recent sedimentation and geochemical characteristics of sediments in Alvarado Lagoon, Veracruz (southwestern gulf of Mexico)| Cronología de la sedimentación reciente y caracterización geoquímica de los sedimentos de la laguna de Alvarado, Veracruz. *Ciencias Marinas*, 40(4), 291-303. Recovered from https://doi.org/10.7773/cm.v40i4.2473

Saxton, K. E., & Rawls, W. J. (2006). Soil water characteristic estimates by texture and organic matter for hydrologic solutions. *Soil Science Society of America Journal*, 70(5), 1569-1578. Recovered from https://doi.org/10.2136/sssaj2005.0117

Shivhare, N., Dikshit, P. K. S., & Dwivedi, S. B. (2018). A comparison of SWAT model calibration techniques for hydrological modeling in the Ganga River watershed. *Engineering*, 4(5), 643-652. Recovered from https://doi.org/10.1016/J.ENG.2018.08.012

Tan, M. L., Gassman, P. W., Srinivasan, R., Arnold, J. G., & Yang, X. (2019). A review of SWAT studies in Southeast Asia: applications, challenges and future directions. *Water*, 11(5), 914. Recovered from https://doi.org/10.3390/w11050914

Verstraeten, G., Lang, A., & Houben, P. (2009). Human impact on sediment dynamics - quantification and timing. *Catena*, 77(2), 77-80. Recovered from https://doi.org/10.1016/j.catena.2009.01.005

Vörösmarty, C. J., Lévêque, C., & Revenga, C. (2005). Fresh waters. In: *Terrestrial environments* (pp. 165-207). Recovered from https://doi.org/10.4324/9780429331183-12

Wang, F., Ge, Q., Yu, Q., Wang, H., & Xu, X. (2017). Impacts of land-use and land-cover changes on river runoff in Yellow river basin for period of 1956-2012. *Chinese Geographical Science*, 27(1), 13-24. Recovered from https://doi.org/10.1007/s11769-017-0843-3

Wang, Y., Jiang, R., Xie, J., Zhao, Y., Yan, D., & Yang, S. (2019). Soil and Water Assessment Tool (SWAT) model: A systemic review. *Journal of Coastal Research*, 93(sp1), 22. Recovered from https://doi.org/10.2112/SI93-004.1

Warrick, J. A. (2014). Trend analyses with river sediment rating curves. *Hydrological Processes*, 29(6), 936-949. Recovered from https://doi.org/10.1002/hyp.10198

Williams, J. R. (2012). The EPIC model. In: Singh, V. (ed.). *Computer models of watershed hydrology* (pp. 909-1000). USA: Water Resources Publications. Recovered from Recovered from https://www.wrpllc.com/books/cmwhn.html

Williams, J. R., & Berndt, H. D. (1977). Sediment yield prediction based on watershed hydrology. *Transactions of the American Society of Agricultural Engineers*, 20(6), 1100-1104. Recovered from https://doi.org/10.13031/2013.35710

Wohl, E., Barros, A., Brunsell, N., Chappell, N. A., Coe, M., Giambelluca, T., Goldsmith, S., Harmon, R., Hendrickx, J. M. H., Juvik, J., Mcdonnell, J., & Ogden, F. (2012). The hydrology of the humid tropics. *Nature Climate Change*, 2, 655-662. Recovered from https://doi.org/10.1038/NCLIMATE1556

Wuthrich, D. (2006). Google Earth Pro. *Geospatial Solutions*, 16, 30-32.

Yang, H. F., Yang, S. L., Xu, K. H., Milliman, J. D., Wang, H., Yang, Z., Chen, Z., & Zhang, C. Y. (2018). Human impacts on sediment in the Yangtze River: A review and new perspectives. *Global and Planetary Change*, 162, 8-17. Recovered from https://doi.org/10.1016/j.gloplacha.2018.01.001